AIAA Modeling and Simulation Technologies Conference and Exhibit
16 - 19 August 2004, Providence, Rhode Island

AIAA 2004-5441

New Predictive Filters for Compensating the Transport Delay on a Flight Simulator

Liwen Guo* and Frank M. Cardullo†
State University of New York at Binghamton, Binghamton, NY 13902

Jacob A. Houck‡
NASA Langley Research Center, Hampton, VA

Lon C. Kelly §
Unisys Corp., Hampton, VA

and

Thomas Wolters **
NASA Langley Research Center, Hampton, VA

The problems of transport delay in a flight simulator, such as its sources and effects, are reviewed. Then their effects on a pilot-in-the-loop control system are investigated with simulations. Three current prominent delay compensators—the lead/lag filter, McFarland filter, and the Sobiski/Cardullo filter were analyzed and compared. This paper introduces two novel delay compensation techniques—an adaptive predictor using the Kalman estimator and a state space predictive filter using a reference aerodynamic model. Applications of these two new compensators on recorded data from the NASA Langley Research Center Visual Motion Simulator show that they achieve better compensation over the current ones.

Nomenclature

t_d	=	transport delay
$\mathbf{\Phi}$	=	state transition matrix
$\mathbf{\Psi}$	=	integral matrix of the state transition matrix
$\mathbf{K}$	=	Kalman gain matrix
$\mathbf{x}_a$	=	aircraft state vector
$\mathbf{x}$	=	filter state vector
$\mathbf{x}_p$	=	predicted filter state vector
y	=	aircraft state output to the visual system
y_p	=	predicted aircraft state output
u	=	control input from the simulator operator
$\tilde{\boldsymbol{\theta}}$	=	Estimation by the Kalman estimator
i	=	time index during simulation
s	=	Laplace operator

* PhD Candidate, Department of Mechanical Engineering, AIAA Member
† Professor, Department of Mechanical Engineering, Associate Fellow AIAA
‡ Asst. Branch Head, Associate Fellow AIAA
§ Software Engineer
** Computer Engineer

I. Introduction

The issues of transport delay on a flight simulator have long been raised and intensively studied. The total transport delay has lessened somewhat due to the development of computer technology, but it still remains a problem on state-of-the-art flight simulators.

The time delay on a vehicle simulator is the time elapsed from an operator's input until an appropriate stimulus is presented to the operator by the associated hardware. It is caused primarily by three sources: sampling delay, processing time and data transfer time. Sampling delay is the time it takes a control input to be sensed by the simulation computer, which samples the operator's control input at the beginning of each computation frame while the control input arrives stochastically, hence the change of input between two consecutive sampling events is delayed. The worst-case scenario is almost a full frame of time delay, and the average sampling delay is a half frame. As the primary source of time delay, the processing time consists of two parts—the time it takes the simulation computer to calculate the aircraft response from the sampled operator's control input, and the time for the computers in the cueing systems to prepare the basic cues. Data transfer time is the time it takes the simulation computer to output signals to the cockpit, motion system, and/or the visual system. If the updating rates of the mainframe computer and the cueing system are not equal and the latter is not an integer multiple of the former, communication asynchrony occurs and results in delay. Asynchronous time delay is a periodic delay[1]. If the transfers are asynchronous, the data transfer delay affects the sampling delay[2]. As long as the transfer time is less than the sampling interval (i. e., the frame length), transfer time may be considered the same as processing time[3]. Although the simulator time delay consists of several components from different subsystems, they make no difference to the operator, who only feels the total effect.

Figure 1 illustrates how an operator controls a simulator with the visual cue as the feedback. The sampling delay happens between the hand and the plant, the processing delay occurs in the plant and between the output and the display, and the delay due to communication asynchrony may arise when there exists an update rate difference between the plant and the display system. If the overall delay reaches a noticeable level, when the operator issues a control command, he will see insufficient response from the display relative to his expectation; hence the operator cognitive control logic makes him maneuver further until the expected display is seen; but because of the delay, the display will show the operator that he has already over controlled, resulting in a compensation or a modification, and so on. This example demonstrates that the immediate effect of long transport delay is a "Pilot Induced Oscillation" (PIO). From this example, the following problems caused by the time delay are expected:

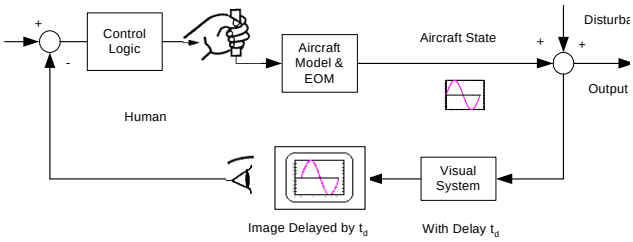

Figure 1. Illustration of a man-machine control system with a visual cue as feedback

- The man-machine system performance is degraded because of the PIO;
- The operator's control workload is increased due to over control and modification;
- The operator's assessment of the handling quality of the system is diminished.

The literature supports the above analyses regarding the effects of transport delay in the man-in-the-loop flight simulator system. Several metrics indicate that transport delay degrades the man-machine system performance. Transport delay increases the system Root Mean Square Error (RMSE) associated with various tasks[4,5]; the Power Spectral Density (PSD) analyses of the operator controls demonstrate that the time delay causes the operator's workload to increase, especially in the high frequencies[6,7]; the Cooper-Harper Rating (CHR) also shows that the operator's handling quality assessment is affected by the delay[8]. Large transport delays may also induce simulator sickness[9].

In fact, the PIO in a flight simulator caused by transport delay indicates that the system converges at a slower speed, or the system stability is taxed. This can be illustrated by modeling a flight simulation task, as shown in Fig. 2. The pilot model, given by Eq. (1), matches a lateral control task performed with a rate controller cascading a delay term representing the lumped neuromuscular and cognitive time delay of the

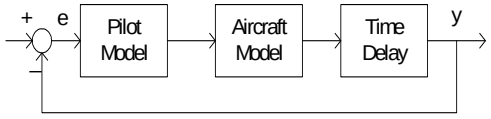

Figure 2. Block diagram of a simulation with a man-in-the-loop control

predictor[10]; the aircraft model, given by Eq. (2) represents the changes of the roll angle per deflection of the control stick, at a flight condition of 430 knots and 30000 feet altitude[11]; and the time delay block refers to the artificially inserted transport delay (denoted by t_d) represented by the 2nd-order Pade approximation (Eq. (3)). Three values of the artificial delay were tried: 0, 200, or 400 ms, and the closed-loop step responses and the open loop frequency responses of these three cases are given in Fig. 3 and Fig. 4.

From the step responses, a time delay of 200 ms makes this control system much more oscillatory than the undelayed system, but the system still converges to the same steady state value, indicating that there is no gain distortion caused by the added delay. When the time delay is 400 ms, the system becomes unstable. The Bode diagrams show that the time delay only introduces phase lag to the system without causing gain distortion. This agrees with the mathematical expression of a pure delay, i.e., $e^{-t_d s}$ (first equality of Eq. (3)), whose magnitude is always unity and phase is negative. The phase lag caused by time delay t_d is given by Eq. (4), where ω_c is the system crossover frequency. When this system suffers 200ms time delay, the phase margin decreases but it is still positive, hence the system is still stable but reaches a steady state value slowly; for 400 ms delay, the phase margin is negative, resulting in an unstable system.

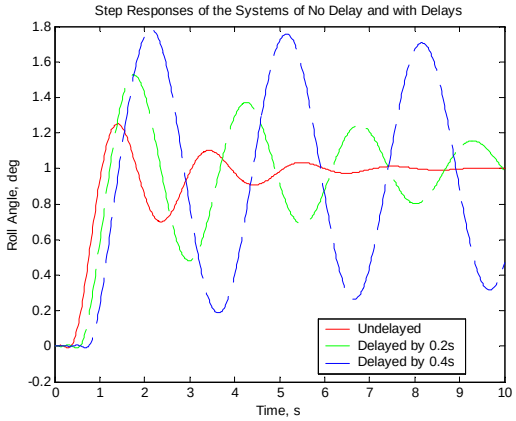

Figure 3. Step responses of a closed loop system with different delays

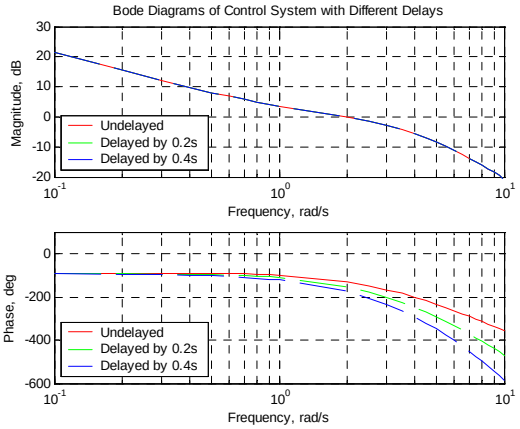

Figure 4. Bode Diagrams of a closed loop system with different delays

$$H_p(s) = \frac{18(s+1)e^{-0.3s}}{(s+3)(s+9)} \tag{1}$$

$$\frac{\varphi(s)}{\delta_e(s)} = 5.57 \frac{\frac{s^2}{3.46} + \frac{0.48s}{1.86} + 1}{s(0.16s+1)\left(\frac{s^2}{3.53} + \frac{0.48s}{1.88} + 1\right)} \tag{2}$$

$$\frac{y_d}{y} = e^{-t_d s} \approx \frac{s^2 - \frac{6}{t_d}s + \frac{12}{t_d^2}}{s^2 + \frac{6}{t_d}s + \frac{12}{t_d^2}} \tag{3}$$

$$\phi_d = t_d \omega_c \tag{4}$$

The impact of time delay on the man-machine system is not only relevant to the amount of the delay, but also relevant to the system dynamics. Specifically, the system bandwidth or crossover frequency affects the impact of

time delay on the system. To illustrate it, time delays were added to a 2nd-order dynamic model with a variable bandwidth, and the system responses were analyzed. The model is given in Eq. (5), in which the damping ratio remains unchanged, but two natural frequencies were used to create two systems with different bandwidths. Some properties of the systems are listed in Table 1.

Figure 5 shows the closed-loop step responses of these two systems with 0, 150 and 300 ms added delays. With zero added delay, system I (upper figure) has slower responsiveness than system II because its bandwidth is lower. However, with a 150 ms delay, system I responds faster than system II, showing that a dynamic system with higher bandwidth tends to be impacted more by the same amount of delay. With a delay of 300 ms, system I becomes more oscillatory but is still stable, whereas system II is no longer stable. Further analysis shows that although the two systems have the same phase margin, system I can tolerate much longer maximal time delay than system II (344 ms vs. 238 ms). This can be interpreted using Eq. (4). Usually, the system with higher bandwidth tends to have higher crossover frequency (ω_c). It follows from Eq. (4) that the system with higher crossover frequency suffers larger phase lag ϕ_d with the same time delay. And because $t_d = \phi_{PM}/\omega_c$, with the same phase margin (ϕ_{PM}), the system with lower crossover frequency tolerates longer delay.

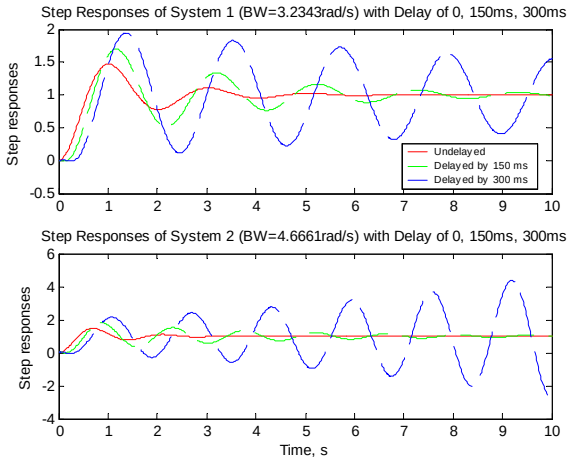

Figure 5. Step responses of the two dynamic systems different delay

Table 1. Properties of two dynamic systems

Properties	System I	System II
Damping ratio	0.33	0.33
Natural frequency (rad/s)	2.259	3.259
Bandwidth (rad/s)	3.2343	4.6661
Crossover frequency (rad/s)	2.8250	4.0755
Phase margin (deg)	55.6599	55.6599
Maximal tolerable delay (s)	0.344	0.238

$$H_{AC}(s) = \frac{\omega^2}{s^2 + 2\zeta\omega s + \omega^2} \tag{5}$$

II. Current Compensation Techniques

Because it causes problems to flight simulations, simulator transport delay must be minimized to reduce its effects. If it is still above some tolerable level, for maintaining desirable simulator performance, algorithms compensating for the delay must be employed. When there exists transport delay in the visual system, what is displayed is the delayed image representing the past aircraft states. Since one cannot generate the undelayed image from the delayed one, the compensation must be directed to the aircraft states. Therefore, the idea of compensation is to predict the future aircraft states making use of the currently available system information so that the image based on the predicted aircraft states can offset the transport delay in the visual system. Such an idea is illustrated in Fig. 6, where in the small plot right after the predictor block the green curve is the prediction.

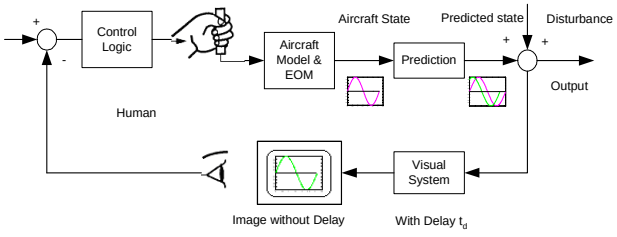

Figure 6. Illustration of the idea of compensating transport delay with a predictor

The predicted green curve in Fig. 6 is an ideal prediction, i.e., it has exactly the same shape as the original magenta one, only with a pure phase shifted forward. The ideal predictor does not exist in the real world. The actual predictor generally introduces error, and the longer the time delay, the greater the error. The mathematics illustrate that pure time delay brings phase lag to the system without changing the magnitude. Therefore, a good predictor must meet two basic criteria: first, it must be able to provide sufficient phase lead to offset the phase lag caused by the time delay; second, it must introduce minimum gain distortion. A third criterion is that the computation workload of the predictor is not heavy and is easy to implement.

Many compensation techniques have been developed to compensate the transport delay in the flight simulator to date; among them the lead/lag filter, the McFarland compensator and the Sobiski/Cardullo state space filter are the three prominent techniques to be considered. The transfer function of the lead/lag is given by

$$\frac{Y_p(s)}{Y(s)} = \frac{s+\omega_n}{s+\omega_d}, (\omega_n < \omega_d) \tag{6}$$

where $Y_p(s)$ and $Y(s)$ are the Laplace transforms of the predicted aircraft state and the undelayed aircraft state, respectively; ω_n and ω_d are the two corner frequencies of the filter. Figure 7 gives the Bode asymptotes of both the magnitude and the phase.

The lead/lag filter provides some phase lead in $[\omega_n\ \omega_d]$, while introducing significant gain distortion in the same frequency interval**.** The phase lead improves the system stability margin, but it may be subjected to high-frequency noise problems. Apart from the gain distortion, the lead/lag filter has poor ability to compensate for long time delays. The design objective is to choose the two corner frequencies so that it provides maximal phase lead at the cost of acceptable gain distortion. The implementation of a lead/lag filter is quite simple. Therefore, the lead/lag compensator does not meet the first two criteria, but it meets the third criterion. As an Infinite Impulse Response (IIR) filter, the lead/lag compensator makes use of the previous prediction to calculate the current prediction, thus the error of one iteration is passed down to the next, resulting in error accumulation. This is the primary reason for the gain distortion.

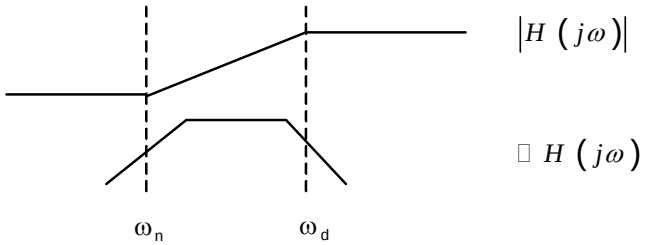

Figure 7. Bode asymptotes of the lead/lag filter

Therefore, Richard McFarland of the NASA Ames Research Center proposed a Finite Impulse Response (FIR) predictive filter to compensate the transport delay[12]. Its pulse transfer function and difference equation are given by

$$y_p(k) = y(k) + b_0 v(k) + b_1 v(k-1) + b_2 v(k-2) \tag{7}$$

where y is the aircraft state to be predicted, v is the corresponding velocity, y_p is the predicted aircraft state, and k is the iteration index. Obviously, the McFarland compensator is a special integrator making use of three consecutive steps of velocity. The three coefficients b_0, b_1 and b_2 determine the ability of compensating the time delay. McFarland uses a method known as sinusoidal tuning to design these three coefficients, which are solutions of three equations derived from the boundary conditions of the "bandpass" $[0\ \omega_0]$ by assuming sinusoidal input to the filter. The bandpass comes from the

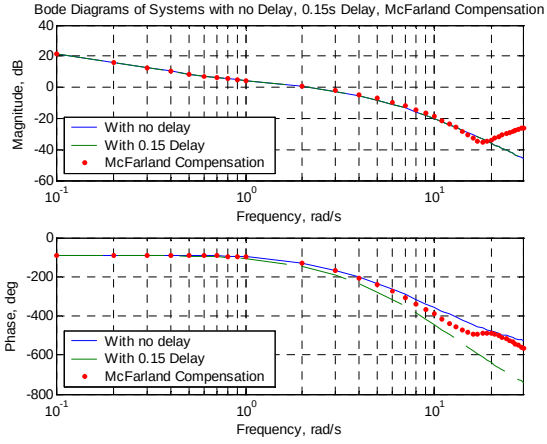

Figure 8. Bode diagram of McFarland compensation

assumption that the pilot operates primarily within this frequency interval and the operation beyond ω_0, about 6-20 rad/s, is small. Simulations show that for time delay up to 150 ms, the McFarland filter provides satisfactory phase compensation when the frequency is below 7 rad/s, but the phase lead is not sufficient in higher frequencies; the gain distortion is small when the frequency is within the bandpass, but the gain distortion escalates when it is beyond the bandpass (Fig. 8). In application of the McFarland compensator to recorded simulation aircraft states, the gain distortion appears as the artifacts in the peak areas and the large spikes (Fig. 9). The problem of these undesirable spikes becomes more serious when time delay is longer. Investigation shows the spikes result because the three McFarland coefficients are constant functions of the time delay, not changing with the aerodynamics or the simulation conditions. Thus, a possible solution to this problem is to design a predictor adaptable to the simulation conditions that substantially reduces the spikes or gain distortions with acceptable computation cost.

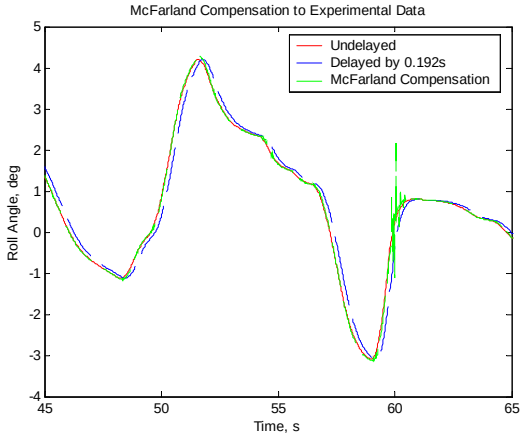

Figure 9. McFarland compensation applied on the recorded roll angle different delays

In 1987, Sobiski and Cardullo[13] proposed a state space predictor for compensating the transport delay. It is based on the equation

$$\mathbf{x}(t+t_d) = e^{\mathbf{A}t_d}\mathbf{x}(t) + \int_0^{t_d} e^{\mathbf{A}(t_d-\tau)}\mathbf{B}u(t+\tau)\,d\tau \tag{8}$$

that is derived from the solution of the state space differential equation $\dot{\mathbf{x}} = \mathbf{A}\mathbf{x} + \mathbf{B}u$. This equation shows that the predicted state vector $\mathbf{x}(t+t_d)$ may be calculated from the current state $\mathbf{x}(t)$ provided that the future input u is known between t and $t+t_d$, an obviously impossible condition with stochastic operator's control input u. Therefore, Sobiski made some assumptions about the form that the input might take, i.e., piece-wise constant, sinusoidal, exponentially decaying, etc, so that the future input may be approximated by the current input. Then the prediction is given by

$$\mathbf{x}(t+t_d) = \left[e^{\mathbf{A}t_d}\right]\mathbf{x}(t) + \left[\int_0^{t_d} e^{\mathbf{A}(t_d-\tau)}d\tau\right]\mathbf{B}u(t) \tag{9}$$

By denoting $\mathbf{\Phi} = e^{\mathbf{A}t_d}$ and $\mathbf{\Psi} = \int_0^{t_d} e^{\mathbf{A}(t_d-\tau)}d\tau$, it is simplified to $\mathbf{x}_p = \mathbf{\Phi}\mathbf{x} + \mathbf{\Psi}\mathbf{B}u$. Directly from Equation [9], the structure of the Sobiski/Cardullo filter is illustrated in Fig. 10. The Sobiski/Cardullo state space predictive filter is an original approach for compensating the time delay. Theoretically it can compensate longer delay than the McFarland compensator because it uses more system information, i.e., the full state vector. The frequency responses show that it introduces smaller gain distortion to the system than the McFarland compensator. However, the Sobiski/Cardullo filter has several problems. First, it only applies to a Linear Time Invariant (LTI) system, while the aerodynamics of a flight simulator is usually nonlinear and time variant, thus the matrices $\mathbf{A}$, $\mathbf{\Phi}$ and $\mathbf{\Psi}$ are not available, and that is why the Sobiski/Cardullo filter has stayed in laboratory use since its advent more than 10 years ago. Second, it has some limitations in Sobiski's implementation. Third, the assumptions for approximating the future control input with the current one do not apply

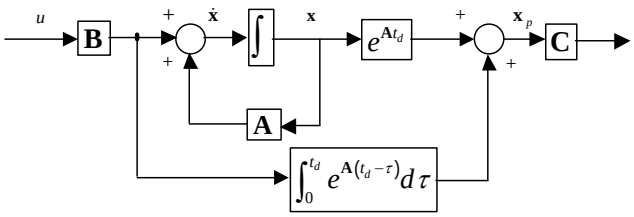

Figure 10. Sobiski/Cardullo compensator

to the real simulation conditions. Finally, the state space filter requires high computation cost because of the matrix operations. Therefore it is worthy to develop the first practical state space predictor that can compensate longer delay than currently available time delay compensators, and simplify the algorithm to provide minimal computation cost.

III. New Developments in Delay Compensation

In order to avoid the problems in the McFarland filter and the Sobiski/Cardullo state space filter, two novel compensation algorithms have been developed—the adaptive predictor that uses a Kalman estimator and the state space predictor that uses a linear model of the aircraft dynamics to predict future states. The well-known Kalman estimator technique is used in a unique manner so that the predictor can provide accurately the desired amount of prediction. From six different algorithms of the Kalman estimator, the ultimate choice was made based on the results of the piloted simulator experiments. The state space filter with a linear reference model is the first practical model reference state space predictor applied in a flight simulator to compensate the time delay. From several currently available linear aircraft dynamic models, one that achieved the best prediction based on the batch tests was chosen. The relation between the reference model and the quality of prediction was also investigated. By simplifying the state predictor to an ordinary predictor in a transfer function format, the computation workload is reduced significantly. The two new compensators are described below.

A. Designing the Adaptive Predictor

An adaptive predictor has been developed with the coefficients of the predictor being changed based on some adaptation mechanism as the simulation proceeds. For convenience of making comparison with the McFarland predictor, three consecutive steps of velocity are also used in the adaptive predictor. The idea is illustrated in Fig. 11, where y is the aircraft state, $y_c = y_d + b_0 v + b_1 v_{-1} + b_2 v_{-2}$ is the compensated aircraft state, where y_d is the delayed aircraft state, and v, v_{-1} and v_{-2} are the velocities of y in three consecutive iterations. The mechanism of adaptation is to minimize the quadratic loss function given by

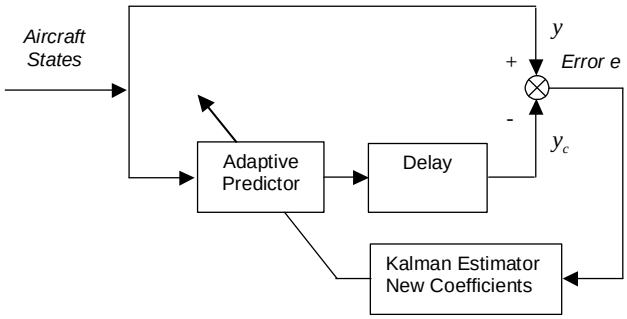

Figure 11. Structure of the adaptive predictor with the Kalman estimator

$$I = \frac{1}{2}\sum_{i=k_0}^{k}\left\{ y(i) - y_c(i) \right\}^2 \tag{10}$$

Minimizing the cost function in Eq. (10) gives rise to left pseudo-inversion of a matrix, and by making use of the Kalman matrix inversion theorem, the solution ends up as

$$\mathbf{K}(k) = \mathbf{P}(k-1)\,\mathbf{j}(k)\left[1 + \mathbf{j}^T(k)\,\mathbf{P}(k-1)\,\mathbf{j}^T(k)\right]^{-1} \tag{11}$$

$$\tilde{\boldsymbol{\theta}}(k) = \tilde{\boldsymbol{\theta}}(k-1) + \mathbf{K}(k)\left[y(k) - y_d(k) - \mathbf{j}^T(k)\,\tilde{\boldsymbol{\theta}}(k-1) \right] \tag{12}$$

$$\mathbf{P}(k) = \left[\mathbf{I}_{3\times 3} - \mathbf{K}(k)\,\mathbf{j}^T(k)\right]\mathbf{P}(k-1) \tag{13}$$

where $\tilde{\boldsymbol{\theta}}(k) = \left[b_0(k) \quad b_1(k) \quad b_2(k) \right]^T$ gives the three coefficients of the adaptive predictor, and $\mathbf{j}^T(k) = \left[v(k) \quad v(k-1) \quad v(k-2) \right]$ is a vector consisting of the three consecutive velocities. The algorithm

starts with $\mathbf{P}(k_0) = \left(\mathbf{j}^T(k_0)\,\mathbf{j}(k_0)\right)^{-1}$ and $\tilde{\boldsymbol{\theta}}(k_0) = \mathbf{P}(k_0)\,\mathbf{j}^T(k_0)\left(y(k_0) - y_d(k_0)\right)$, where k_0 corresponds to the first time when quantity $\mathbf{j}^T(k_0)\,\mathbf{j}(k_0)$ is nonsingular. Notice that since the quantity inside the brackets is a scalar, the matrix inversion is avoided, and the algorithm can be implemented in real time. Simulations show that the new adaptive predictor substantially reduces the high frequency gain distortion and spikes caused by the McFarland filter.

The performance of the algorithm may be improved by introducing an exponential forgetting factor to the cost function because the simulation condition is time varying. Apart from the Kalman estimation algorithm with the forgetting factor, three other simplified least-square algorithms were also tried. The simplification comes from avoiding updating the matrix $\mathbf{P}$, since updating matrix $\mathbf{P}$ dominates the computing effort for large number of iterations. Because the recursive least-square algorithm updates the current estimate $\boldsymbol{\theta}^T(k)$ based on the previous estimate $\tilde{\boldsymbol{\theta}}(k-1)$ and the new measurement $y(k) = \mathbf{j}^T(k)\boldsymbol{\theta}(k)$, which contains information only in the direction $\mathbf{j}^T(k)$ in the parameter space, Kaczmarz[14] proposed the normalized projection algorithm that minimizes $\left|\tilde{\boldsymbol{\theta}}(k) - \tilde{\boldsymbol{\theta}}(k)\right|^2$ subject to the constraints, $y(k) = \mathbf{j}^T(k)\tilde{\boldsymbol{\theta}}(k)$. The cost function for the Kaczmarz's algorithm (the normalized projection) is $I = \left|\tilde{\boldsymbol{\theta}}(k) - \tilde{\boldsymbol{\theta}}(k)\right|^2 + \bar{\alpha}\left[y(k) - \mathbf{j}^T(k)\tilde{\boldsymbol{\theta}}(k)\right]$, which may be considered as a function of vector variable $\boldsymbol{\theta}(k)$ with $\bar{\alpha}$ the Lagrange multiplier as a parameter. Taking derivatives with respect to $\boldsymbol{\theta}(k)$ and $\bar{\alpha}$ and invoking the stationary results in the Kaczmarz's algorithm. The Kaczmarz's algorithms may be modified to the Stochastic Approximation (SA) algorithm, given by Eq. (14), which is tolerable to random noise in the input data y and $\mathbf{j}^T$. A further simplification is the Least Mean Square (LSM) algorithm, which is the simplest algorithm. In order to compare the performance of the McFarland predictor and the above five versions (the basic Kalman estimator, Kalman estimator with forgetting factor, the Kaczmarz's algorithm, the SA algorithm and the LSM algorithm) of the adaptive filter, three criteria were used: a) the phase difference between the undelayed aircraft state y and the compensated aircraft state y_c, b) error index defined by Eq. (10), and c) magnitude of spikes. Note that these three criteria are not independent of each other, e.g., criteria a) and c) affect criterion b). Comparisons of simulations with all these criteria show that the Stochastic Approximation algorithm is superior to the other four versions of the adaptive predictor and the McFarland filter.

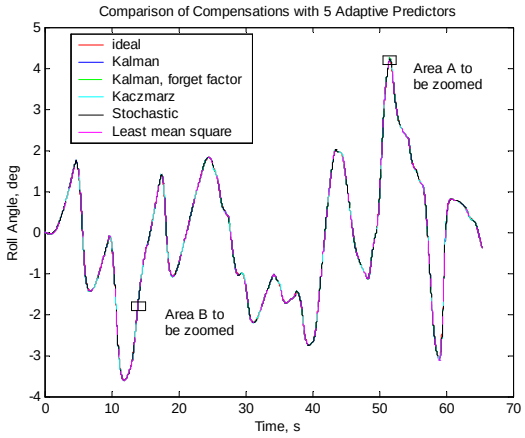

Figure 12. Adaptive compensation applied on the recorded roll angle different delays.

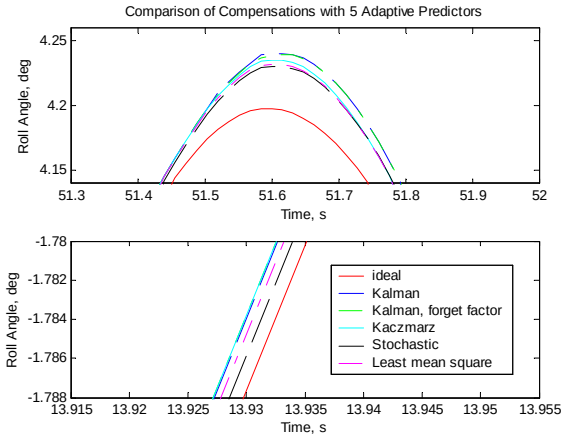

Figure 13. Zoom of Figure 12

Figure 12 illustrates results of compensation employing the five versions of the adaptive predictors on recorded simulator roll angle. In this figure the term "ideal" in the legend refers to the case where the visual delay is zero. Because the prediction errors and differences among these algorithms are small compared with the scale of the roll angle, a peak area in Fig. 12 is zoomed in Fig. 13, which clearly shows that all revised adaptive algorithms are superior to the original Kalman estimator, and the Stochastic Approximation algorithm causes the least predicting error among all. It agrees with the analysis of error index defined by Eq. (10)) (See Table 2).

$$\boldsymbol{\theta}(k) = \boldsymbol{\theta}(k-1) + \frac{\mathbf{j}(k)\left[y(k) - y_d(k) - \mathbf{j}^T(k)\boldsymbol{\theta}(k-1) \right]}{\sum_{i=1}^{k} \mathbf{j}(i)\mathbf{j}^T(i)} \tag{14}$$

Therefore, the stochastic approximation algorithm will be chosen to be the adaptive predictor that will be used on the NASA Langley Research Center Visual Motion Simulator. As stated in the previous section, the McFarland brings large spikes while providing phase lead (Fig. 9). The adaptive predictor significantly reduces the spikes and the zigzags in the peak areas caused by the McFarland filter, and a comparison between the McFarland filter and the adaptive predictor with the stochastic approximation algorithms is illustrated in Fig. 14.

Table 2. Prediction error index of the five adaptive algorithms

Algorithms	t_d =0.1 s	t_d =0.2 s
Kalman	1.3540	18.9492
Kalman (forget factor)	1.2984	18.2382
Kaczmarz	1.2101	15.9925
Stochastic approximation	0.8334	7.8981
Least mean square	1.0511	11.4920

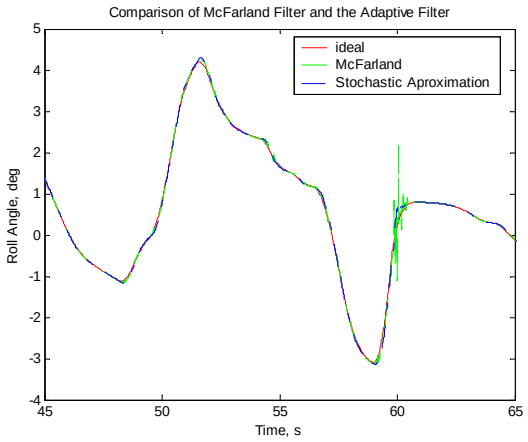

Figure 14. Comparison between the McFarland filter and the adaptive predictor

B. A Practical State Space Compensator

The state space prediction equation $\mathbf{x}_p = \boldsymbol{\Phi}\mathbf{x} + \boldsymbol{\Psi}\mathbf{B}u$ is based on a Linear Time Invariant (LTI) system, and cannot be implemented directly in a flight simulator to compensate the time delay because the simulated aircraft dynamics are usually nonlinear, time-variant and coupled in different degrees of freedom. Instead of being expressed in state space equations, they are often expressed in coupled non-linear differential equations. Employing an aircraft reference model in the predictor algorithm can solve this problem. A reference model is an approximate linear aircraft dynamics model that is used to form the predictor states from the operator control input and the aircraft states, as well as to provide the state transition matrix and the convolution integral, so that the state space prediction equation $\mathbf{x}_p = \boldsymbol{\Phi}\mathbf{x} + \boldsymbol{\Psi}\mathbf{B}u$ may be applied in a flight simulator when the aircraft state is not measurable. Figure 15 illustrates this approach, where $\mathbf{x}_a$ is the aircraft state vector, $\mathbf{x}$ is the filter state vector and $\mathbf{x}_p$ is the predicted filter state vector. Because the aircraft state vector $\mathbf{x}_a$ includes the aircraft state y to be predicted and its velocity and acceleration, the filter state vector $\mathbf{x}$ is also in terms of y. Therefore, the predicted filter state $\mathbf{x}_p$ calculated with $\mathbf{x}_p = \boldsymbol{\Phi}\mathbf{x} + \boldsymbol{\Psi}\mathbf{B}u$ contains the predicted information of y. Then use the matrix $\mathbf{C}$ to retrieve y_p, and the prediction is achieved.

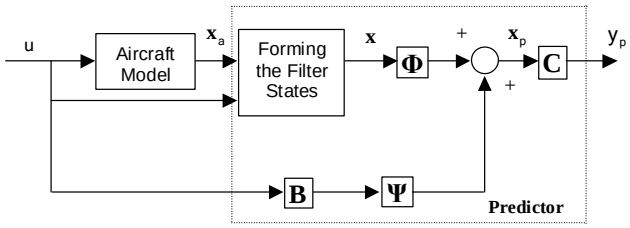

Figure 15. Structure of the state space compensator using a reference model

Four 4th-order reference models were tried first. The first two models give the relation of the pitch angle and the roll angle, respectively, and the corresponding stick deflections of a fixed wing jet flying at an altitude of 30,000ft

and an airspeed of 430 knots. They will be called Model One and Model Two (Eq. (2)). The other two models are Boeing 757 pitch models, one for cruise, and one for landing. They will be called Model Three and Model Four. These four models share the same general form of transfer function

$$H_{AC}(s) = \frac{\beta_2 s^2 + \beta_1 s + \beta_0}{s^4 + \alpha_3 s^3 + \alpha_2 s^2 + \alpha_1 s + \alpha_0} \tag{15}$$

The observable state space matrices of this general model are given in Eq. (16). Selection of the observable canonical form is made because the output is desired to be the first state variable. The expressions of the four state filter variables are directly derived from $\begin{cases} \dot{\mathbf{x}} = \mathbf{A}\mathbf{x} + \mathbf{B}u \\ y = \mathbf{C}\mathbf{x} + \mathbf{D}u \end{cases}$, and the result is given in Eq. (17). The four filter state variables are in terms of y, the aircraft state to be predicted, $\dot{y}$, $\ddot{y}$ and u, the input. Then calculate the matrices $\mathbf{\Phi} = e^{\mathbf{A}t_d}$ and $\mathbf{\Psi} = \int_0^{t_d} e^{\mathbf{A}(t_d-\tau)} d\tau$, and implement the algorithm of prediction according to the structure in Fig. 15.

$$\mathbf{A} = \begin{bmatrix} -\alpha_3 & 1 & 0 & 0 \\ -\alpha_2 & 0 & 1 & 0 \\ -\alpha_1 & 0 & 0 & 1 \\ -\alpha_0 & 0 & 0 & 0 \end{bmatrix}, \mathbf{B} = \begin{bmatrix} 0 \\ \beta_2 \\ \beta_1 \\ \beta_0 \end{bmatrix}, \mathbf{C} = \begin{bmatrix} 1 & 0 & 0 & 0 \end{bmatrix}, \mathbf{D} = 0 \tag{16}$$

$$\begin{cases} x_1 = y \\ x_2 = \dot{y} + \alpha_3 y \\ x_3 = \ddot{y} + \alpha_3 \dot{y} + \alpha_2 y - \beta_2 u \\ x_4 = \beta_0 \int_0^T u dt \end{cases} \tag{17}$$

The analysis of compensation on a recorded simulation roll angle with the state space predictors using the four reference models is illustrated in Fig. 16 and Fig.17 (Zooms of Fig. 16). Both the upper and lower subplots of Fig. 17 show that Model Four, the Boeing 757 landing pitch model, achieves the best compensation, that is, the black curve is closest to the undelayed red curve. Table 4 is the result of analysis of the error index defined by Eq. (10). Though Model Three brings slightly smaller squared error sum than Model Four, the phase compensation shows Model Four causes less phase prediction error. Since the phase compensation is more important in considering time delay compensation, Model Four is finally chosen as the refence model for the future state space filter to be applied on the Langley Visual Motion Simulator.

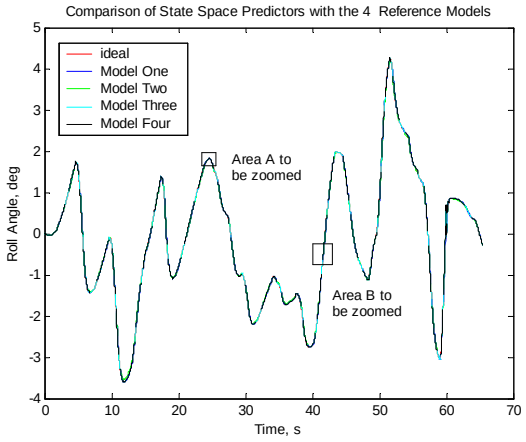

Figure 16. Comparison between the McFarland filter and the adaptive predictor

Finally, the McFarland compensator, the adaptive predictor using the stochastic approximation algorithm and the state space predictor using the Boeing 757 landing pitch model were compared in terms of the error index, and the result is given in Table 5. Both novel predictors cause less compensation error than the McFarland filter and the state space filter causes the least.

Table 4. Prediction error index by state space predictors with the four reference models

Reference models	t_d =0.1 s	t_d =0.2 s
Model One	0.0811	2.5530
Model Two	0.1356	4.4756
Model Three	0.0633	1.8215
Model Four	0.0649	1.9497

Table 5. Prediction error index by the McFarland, adaptive and state space predictors

Compensators	t_d =0.1 s	t_d =0.2 s
McFarland filter	0.5973	12.051
Adaptive predictor	0.5819	7.3387
State space predictor	0.0649	1.9497

C. Simplification and Essence of the State Space Compensator

Calculating the four predicted filter states as given by $\mathbf{x}_p = \mathbf{\Phi x} + \mathbf{\Psi B}u$ involves many matrix operations. However, what is really needed is the predicted aircraft state y_p given by $y_p = \mathbf{C}\mathbf{x}_p$, and because $\mathbf{C} = \begin{bmatrix} 1 & 0 & 0 & 0 \end{bmatrix}$, y_p is just the first element of $\mathbf{x}_p$. Therefore, calculation of the last three elements of $\mathbf{x}_p$ is not necessary; this shows that the algorithm can be simplified. The final simplified state space compensator is given in Eq. (16), where ϕ_{ij} and ψ_j are elements of matrices $\mathbf{\Phi}$ and $\mathbf{\Psi}$.

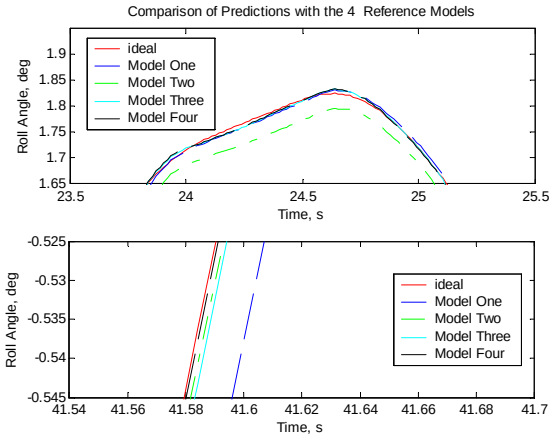

Figure 17. Zoom of Figure 16

$$y_p = \left(\phi_{11} + \phi_{12}\alpha_3 + \phi_{13}\alpha_2\right) y + \left(\phi_{12} + \phi_{13}\alpha_3\right) \dot{y} + \phi_{13}\ddot{y} + \left(\psi_1 - \phi_{13}\beta_2\right) u + \phi_{14}\beta_0 \int_0^T u dt \tag{16}$$

This is the essence of the state space filter! Compared with the McFarland filter, it shows that while the McFarland filter uses three consecutive steps of velocity to predict, the state space filter uses the current velocity, acceleration, the input and its integral to predict.

The coefficients of the terms involving the control input u are so small compared with those of other terms that terms with u may almost be neglected. In other words, a good reference model attenuates the contribution of the second term of $\mathbf{x}\left(t + t_d\right) = e^{\mathbf{A}t_d}\mathbf{x}\left(t\right) + \int_0^{t_d} e^{\mathbf{A}\left(t_d - \tau\right)}\mathbf{B}u\left(t + \tau\right)d\tau$, on which the state space predictor is based. Trivial contribution of input u is a more justifiable reason for approximating the future input with the current one than Sobiski's assumptions. On the other hand, a small contribution of the control input u is desirable because its high frequency jumps are attenuated.

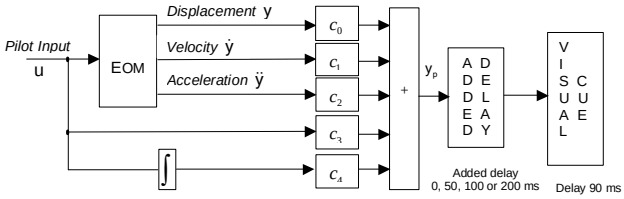

Figure 18. Implementation of the state space compensator using a reference model

The prediction of the state space filter depends solely on the five coefficients in Eq. (16), which are functions of the time delay and the reference model. Therefore, the algorithm based on the state transition matrix and convolution integral with a reference model is only a design tool—to design the coefficients of the compensator. Because the reference model is time invariant, these coefficients are constants that may be calculated offline; in each iteration, only five multiplications and four additions are required—computation is simplified significantly. The state space filter may be implemented as

depicted in Fig. 18, where the 90 ms of delay in the visual system is the baseline transport delay determined in the Visual Motion Simulator at the NASA Langley Research Center, and the coefficients are given in Table 6.

Table 6. Expressions of the State Space Predictors

ϕ_j and ψ_j are elements of matrices $\mathbf{\Phi}$ and $\mathbf{\Psi}$, and α's & β's are the same as defined in Eq. (15)

Coefficient	Expression
c_0	$\phi_{11} + \phi_{12}\alpha_3 + \phi_{13}\alpha_2$
c_1	$\phi_{12} + \phi_{13}\alpha_3$
c_2	ϕ_{13}
c_3	$\psi_1 - \phi_{13}\beta_2$
c_4	$\phi_{14}\beta_0$

IV. Conclusion

The paper presented a brief summary of a systematic study of transport delay in a flight simulator, which included a literature study, basic analyses, measurement, review of current compensators, and the design of two novel compensation techniques. By presenting the results of off-line tests of these two novel compensators on the recorded simulation roll angle, it shows that they achieve better compensation over the McFarland filter with slightly increased computation workload. Both gain distortion and phase error of the compensation are reduced. The State Space Predictor was shown to yield the least error.

The two novel compensators are to be applied in the Visual Motion Simulator at the NASA Langley Research Center to collect data for relevant analyses, in order to evaluate the compensation effectiveness and make comparison with the current prominent compensators.

References

[1] McFarland R. E., "CGI Delay Compensation", NASA TM 86703. NASA Ames Research Center, Jan.1986

[2] Galloway, R. T., & Smith R. B, "Cue Synchronization Measurement Using the Piloted Frequency Sweep Technique", Proceedings of the 17th I/ITSEC, Nov 13-16, pp 786-196, 1995

[3] Cardullo, F. M., & George, G, "Transport Delay Compensation: An Inexpensive Alternative to Increase Image Generator Update Rate", Proceedings of the AIAA Flight Simulation Technologies Conference Washington, DC: American Institute of Aeronautics & Astronautics, AIAA-3564, 1993

[4] Riccio, G., E., Cress, J., D., and Johnson, W., V., "The Effects of Simulator Delays on the Acquisition of Flight Control Skills: Control of Heading and Altitude", Proceedings of the Human Factors Society - 31st Annual Meeting, Santa Monica, CA, 1987

[5] Bailey, R., E., Knotts, L., E., Horowitz, S., J., and Malone, H., L., "Effect of Time Delay on Manual Flight Control and Flying Qualities During In-flight and Ground-based Simulation", Proceedings of the AIAA Flight Simulation Technologies Conference, Washington, DC, AIAA-2370, 1987

[6] Middendorf M. S., Lusk S. L., "Power Spectral Analysis to Investigate the Effects of Simulator Time Delay on Flight Control Activity", Armstrong Aerospace Medical Research Laboratory, 1990 (AIAA-90-3127-CP)

[7] Guo, L., Cardullo, Telban, J., R., Houck, J., A., Kelly, L., C., "The Results of a Simulator Study to Determine the Effects on Pilot Performance of Two Different Motion Cueing Algorithms and Various Delays, Compensated and Uncompensated", AIAA-5676, 2003

[8] Cooper G. E. and Harper R. P. Jr., "The use of Pilot Rating in the Evaluation of Aircraft Handling Qualities", NASA TN D-5153, April, 1969
[9] Zaychik, K., B., and Cardullo, F., M., "Simulator Sickness: the Problem Remains", AIAA Flight Simulation Technologies Conference, AIAA-5526, 2003
[10] Sobiski, D. J., "Predictive Compensation of Visual System Time Delays", Master Degree Thesis, Mechanical Engineering Department, State University of New York at Binghamton, 1988
[11] Ricard, G.L., and Harris, W.T., "Lead/lag Dynamics to Compensate for Display Delays", *Journal of Aircraft, 17,* 212-217, 1980
[12] McFarland R.E., "Transport Delay Compensation for Computer-Generated Imagery Systems", NASA Ames Research Center, NASA-TM-100084, 1988
[13] Sobiski, D., J., and Cardullo, F., M., "Predictive Compensation of Visual System Time Delays", Proceedings of the AIAA Flight Simulation Technologies Conference, Washington, DC, AIAA-2434, 1987
[14] Astrom K. J. and Wittenmark B, "Adaptive Control", Pearson Education, New York, 2001, Chapter 2.